Proceedings of the 21st ICSMGE, Vienna, Austria, 14 – 19 June 2026. Pistrol, Adam & Schweiger (eds.)
Published by: ÖGG, Austrian Society for Geomechanics, Salzburg, Austria, ISBN 978-3-9503898-4-5
https://doi.org/10.53243/ICSMGE2026-159

Assessing the seismic behaviour of a sandy copper tailings with non-uniform shaking events in a novel biaxial shaking table

Arturo Jimenez
Mine Waste, WSP, Perth, WA, Australia, (formerly at UNSW Sydney), Arturo.jimenez@wsp.com

Adrian Russell
School of Civil and Environmental Engineering, UNSW Sydney, Sydney, NSW, Australia

Rohit Tiwari
Technical Design and Engineering, Transport for New South Wales, Parramatta, NSW, Australia (formerly at UNSW Sydney)

ABSTRACT: This paper investigates the liquefaction susceptibility of sandy copper tailings subjected to various non-uniform, biaxial shaking events using a shaking table. Controlled cyclic loadings, simulating seismic events, are applied to examine the liquefaction response of the tailings. Cone penetration testing (CPT) was performed on tailings samples within a calibration chamber and directly in the tailings on the shaking table to establish correlations with the Cyclic Stress Ratio (CSR), a key parameter for predicting liquefaction potential. Laboratory experiments, including triaxial and cyclic simple shear tests, were also conducted to characterise the mechanical properties of the tailings and provide a basis for interpreting the shaking table results within a critical state soil mechanics framework. The timing of liquefaction is used to assess CSR, enabling investigation of their relationship with the observed liquefaction behaviour. The findings of this study provide valuable insights into the liquefaction behaviour of sandy tailings under complex, biaxial shaking conditions, offering practical tools for engineers in the design and mitigation of liquefaction hazards in tailings storage facilities.

KEYWORDS: Soil dynamics, Shaking table experiment, Cone penetration testing, Tailings, Critical state framework.

1 INTRODUCTION

Tailings, waste products generated from mining and mineral extraction operations, pose significant environmental and safety challenges. Stored within tailings storage facilities (TSFs), these mixtures of water and soil-sized particles can undergo a phenomenon known as liquefaction, where they transition from a solid-like material to a fluid-like state with reduced strength due to undrained shearing or internal fabric collapse. Liquefaction can lead to catastrophic TSF failures, causing devastating consequences for human lives, property, and the environment. Recent examples, such as the Merriespruit (1994), Fundão (2015), and Brumadinho (2019) failures (Fourie et al. 2001; Robertson et al. 2019), highlight the urgent need for improved understanding and mitigation of tailings liquefaction.

Liquefaction susceptibility of cohesionless soils has been examined extensively using shaking table tests. Soil stiffness, excess pore pressure, settlement of the soil specimen, re-liquefaction resistance, effect of pre-shaking and shaking history on the liquefaction resistance, and interaction of geotechnical structures and liquefiable soils have been studied (Koga & Matsuo 1990; Zeghal et al. 1999). Shaking history and pre-shaking occurrence have shown to increase the soil strength, CPT penetration resistance and liquefaction resistance under mild and moderate shaking events (Darby et al. 2019).

The timing of liquefaction has been an unaddressed aspect in the assessment of liquefaction hazards, however. This research examines the importance of the timing of liquefaction using UNSW's biaxial shaking table (Tiwari et al. 2024) and beds of a sandy copper tailings. It presents relevant data and correlations that can be used to understand and explore liquefaction timing. It also shows how this information can be assessed to enhance predictions concerning the repercussions of liquefaction events in sandy tailings. First the experimental methodology, including setup of the shaking table tests, instrumentation and sample preparation will be provided. The results will be shown along with the data analysis conducted and liquefaction criteria. The results will then be analysed and integrated with cyclic direct simple shear test (CDSS) results to correlate CRR and the state parameter ψ. CRR is used to assess the liquefaction susceptibility of the copper tailings. The underlying theory behind this approach is explained and the calculations to establish their relationships to ψ are shown.

2 EQUIPMENT

2.1 *UNSW's biaxial shaking table*

Shaking table tests were carried out employing a new type of biaxial shaking table manufactured in Sydney, Australia, which has been commissioned and is fully operational at The University of New South Wales. The top plate of that particular table is 1500×1500 mm in size. It is able to subject three-ton models to regular sine wave time histories involving nominal peak accelerations of ±0.6 g and ±0.4 g in horizontal and vertical directions, respectively. All the design specifications can be found in Tiwari et al. (2024).

2.2 *Laminated shear stack*

Results and measurements from a series of tests on a tailings bed in a laminated shear stack on the shaking table are used to demonstrate its liquefaction susceptibility.

Figure 1 shows a photograph of the shear stack mounted to the shaking table. The shear stack comprises ten identical hollow rectangular laminas made of aluminium. The inside dimensions of each lamina include a 1.5 m length, 0.65 m width and 0.15 m depth. Ten laminae are placed above each other, with a 5 mm gap between each, and between the bottom laminae and the shear stack base, so the total internal depth of the shear stack is 1.55 m. A 10 mm thick vulcanised rubber liner contains the tailings model. The liner prevents tailings or water from passing through the gaps between the laminae. A model inside the shear stack can then be no larger than 1.48 m long, 0.63 m wide and 1.54 m high.

Figure 1. Laminated shear stack placed on the biaxial shaking table at UNSW.

3 MATERIAL AND MODEL PREPARATION

3.1 *Material*

A sandy copper tailings was used inside the laminated shear stack. Index properties of the copper tailings are listed in Table 1 and its particle size distribution is shown in Figure 2.

Table 1. Index properties of copper tailings

Parameter	Symbol	Value	Unit
Specific Gravity	G_s	2.68	
Maximum void ratio	e_{max}	0.89	
Minimum void ratio	e_{min}	0.51	
Median particle size	D_{50}	0.48	mm
Uniformity coefficient	C_u	3.69	
Coefficient of curvature	C_c	1.12	

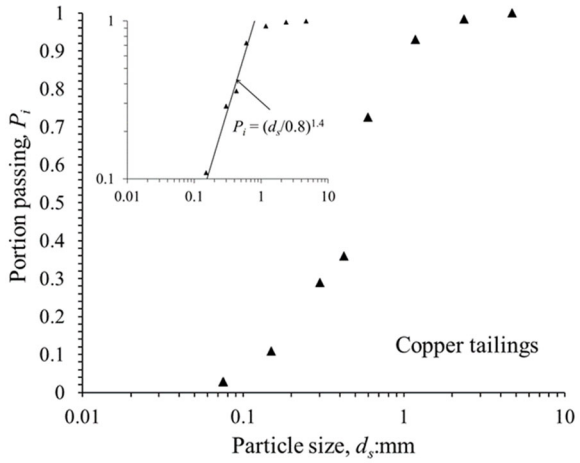

Figure 2. Particle size distribution of the copper tailings.

3.2 *Model preparation*

Two models were prepared and tested using a similar instrumentation configuration as shown in Figure 3. Accelerometers (A), piezometers (P) and laser sensors (L) are positioned as shown in Figure 3. Both accelerometers and piezometers were placed in the middle of the laminated shear stack and spaced 100 mm from one another vertically. By being in the middle, they are least affected by boundary conditions (Zeghal et al. 1999).

In the first model, the tailings bed was placed in layers using the wet pluviation method, achieving a saturated state, and a saturated unit weight and e of 19.2 kN/m^3 and 0.76, respectively. The copper tailings with a water content of 3.5% was dropped through a sieve, with openings of 15 mm x 15 mm, into a free water layer with a depth of approximately 120 mm inside the laminated shear stack. The sieve was moved from left to right inside the shear stack to ensure a homogeneous final height of 100 mm in the first layer of saturated tailings. After the first layer was formed, the surface was levelled and smoothed before positioning accelerometers and piezometers in the middle of the shear stack. The water level was then increased until it reached 120 mm above the first tailings layer and the sieve was readjusted to be 300 mm above the new water layer. Similar steps were carried out for every single layer until a final height of 0.67 m was achieved. Accelerometers and piezometers were placed on top of each of the first four layers.

The second model was deposited in layers and in a partially saturated condition, achieving a unit weight and e of 17.82 kN/m^3 and 0.89, respectively. The deposition method and instrumentation followed a similar procedure to the first model without the free layer of water. After the second model was finished, the achieved saturation degree, S_{r0}, was 85% and the final height was 0.72 m.

Since the initial height of the tailings models were 0.67 m and 0.72 m, both models interacted with the bottom five laminae only. Displacements of selected shear stack laminae were measured using three laser sensors, attached to an end support frame, as shown in Figure 3.

Once the tailings sample is prepared and ready for testing within the shear stack apparatus the laminated shear stack is placed on top of the biaxial shaking table as shown in Figure 1. The base of the shear stack is securely fastened to the shaking table using bolts to prevent movement during testing. Piezometers and accelerometers are then connected to a data logger for signal acquisition.

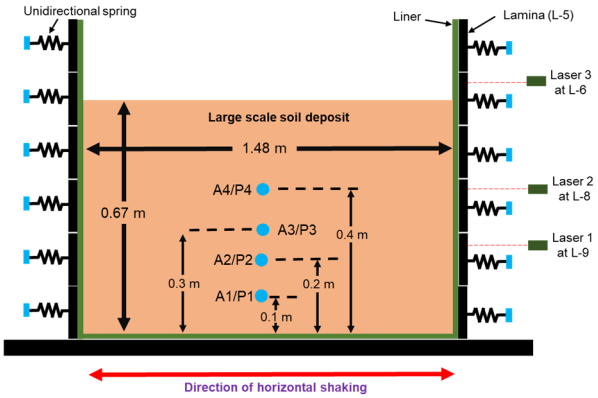

Figure 3. Tailings bed inside the laminated shear stack.

4 SHAKING TABLE EXPERIMENTAL PROGRAM AND RESULTS

4.1 *Shaking table pulses*

Different acceleration pulses were used to excite the shaking table platform, these were generated using the procedure suggested by Yazdandoust (2017). Equation (1) depicts the input acceleration ($A(t)$) versus time (t) for a pre-determined excitation frequency (f).

$$A(t) = \ddot{U}(t) = \sqrt{\beta_1 e^{-\beta_2 t} t^{\xi}} \sin(2\pi f t) \quad (1)$$

The coefficients β_1, β_2 and ξ collectively govern the amplitude, shape and decay of the input acceleration, including the peak ground acceleration (PGA) and its time of occurrence. Their values apply when t is in seconds, f is in Hz and A is in m/s^2. The coefficients used here, which achieve a range of PGAs from 0.08 g to 0.3 g, are presented in Table 2. The f was 2 Hz for PGAs of 0.08 g and 0.1 g, and for the other PGAs the f was 3 Hz.

Table 2. Details of parameters used to generate input pulses.

PGA	Coefficient values			Excitation frequency (f)
	β_1	β_2	ξ	
0.08 g	0.38	1.3	4	2 Hz
0.1 g	0.6	1.3	4	2 Hz
0.12 g	0.85	1.3	4	3 Hz
0.14 g	1.16	1.3	4	3 Hz
0.16 g	1.52	1.3	4	3 Hz
0.2 g	2.4	1.3	4	3 Hz
0.3 g	5.4	1.3	4	3 Hz

4.2 *Accelerations*

Acceleration, $a(t)$, data from both models were filtered using a fourth-order Butterworth lowpass filter with corner frequency of 10 Hz eliminating high frequency noise. This corner frequency was selected based on accelerometer sensibility and previous shaking table tests experience.

Figure 4 and Figure 5 show the horizontal acceleration time histories captured by the accelerometers placed inside the tailings at different depths for PGAs 0.12 g and 0.20 g, respectively. For PGAs below 0.12 g, where liquefaction did not occur, the difference between the top and bottom acceleration (A1 and A4 readings, respectively) records is minimal. From PGA 0.14 g and above, acceleration differences become greater and liquefaction occurs in the upper layers first due to higher shear strains.

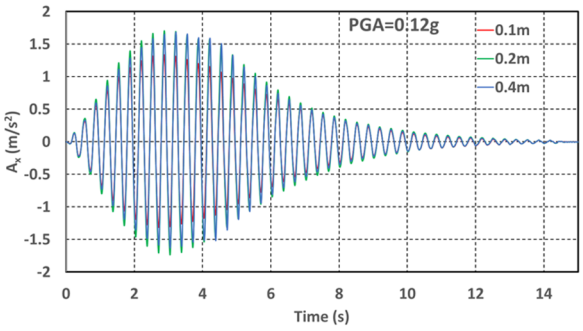

Figure 4. Acceleration time history at different depths of tailings bed in the first model when excited using a PGA of 0.12 g.

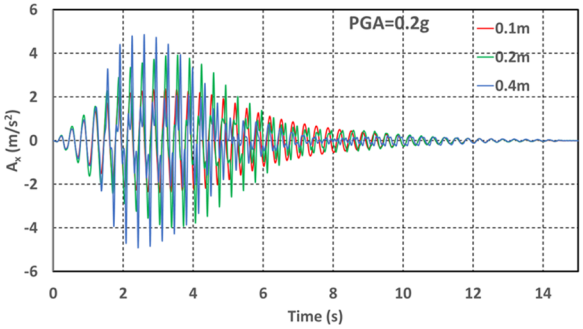

Figure 5. Acceleration time history at different depths of tailings bed in the first model when excited using a PGA of 0.20 g.

4.3 *Pore pressure generation*

During the biaxial shaking events, the pore water pressure, u, exhibited fluctuations in the two tailings models. u, can be decomposed into its initial hydrostatic component, $u_0 = \gamma_w z$, and the excess pore pressure induced by the shaking, Δu. Here, γ_w represents the unit weight of water and z denotes the depth.

The pore pressure starts from the hydrostatic level and builds up rapidly during the seismic shaking event approaching its peak value within several loading cycles based on the induced shaking pulses in Table 2. After its peak value, u starts to decrease as Δu dissipates, displaying pronounced fluctuations throughout the remainder of the shaking event. $a(t)$ peaks and u peaks did not occur at the same time.

4.4 *Pore pressure time histories*

The pore water pressure response was retrieved by piezometers P1, P2, P3 and P4 distributed along the depth as shown in Figure 3. For brevity, only time histories of u readings from P1 and P4 at a PGA of 0.14 g are shown in Figure 6 for the first model. All time histories for the first and second models can be found in Jimenez (2024). Horizontal dashed lines reflecting excess pore pressure ratios, r_u, equal to 0.9 are also shown. r_u here is the ratio between Δu and the effective vertical stress, σ'_v, that is $\sigma'_v = \sigma_v - u$. Thus, when $r_u = 1$ then $\Delta u = \sigma'_v$ and $u = \sigma_v$. Here, liquefaction occurs when $r_u \geq 0.9$ meaning that $\sigma'_v \approx 0$ at different depths in the tailings model. This definition of r_u finds frequent application within the context of cyclic shear tests and shaking table tests related to the liquefaction susceptibility of sandy soils (Koga & Matsuo 1990; Zeghal et al. 1999).

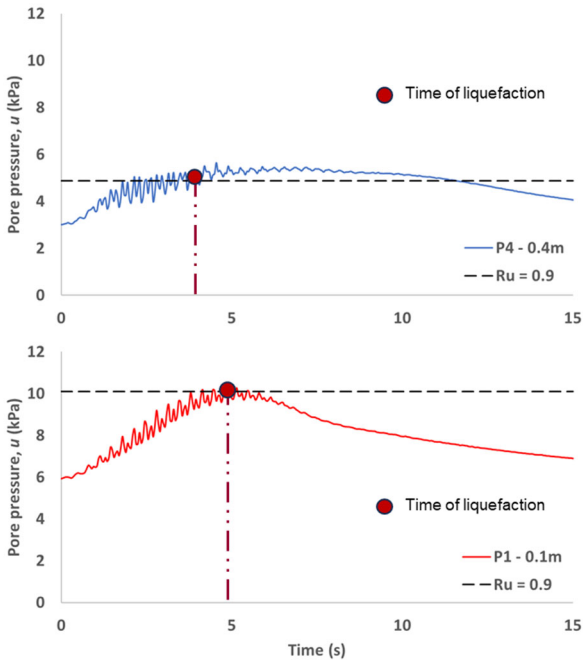

Figure 6. Pore water pressure, u, time histories from P1 and P4 in the first model with a PGA 0.14 g.

The observation of post-shaking pore pressures not totally returning to their initial hydrostatic conditions, u_0, across all monitored layers where liquefaction occurs suggests minor subsidence of the piezometers induced by the seismic events. This vertical displacement of the piezometer tip translates to an increase in total vertical stress at the tip elevation relative to its pre-shaking value in each shaking event. The piezometer tips in the second model exhibit considerably larger vertical displacements during liquefaction, especially in seismic events

of greater intensity, i.e. PGA 0.14 g to 0.30 g. This phenomenon can likely be attributed to the looser initial density of the soil sample.

Seismic excitations with peak ground accelerations (PGAs) of 0.08 g and 0.10 g did not induce liquefaction in the tailings layers of either Model 1 or Model 2. A PGA of 0.12 g resulted in liquefaction of the upper tailings layer (P4) in Model 1, while the lower layer (P1) remained unaffected. However, this same seismic event triggered liquefaction throughout the tailings deposit in Model 2. Both models experienced liquefaction in all tailings layers when subjected to a PGA of 0.14 g or greater as observed in Figure 6. The data obtained from piezometers P1, P2, P3 and P4 further revealed variations in the timing of liquefaction at different depths within the tailings models, highlighting the importance of the timing of liquefaction in the liquefaction susceptibility assessment developed in this study for the copper tailings.

5 CONE PENETRATION RESISTANCES

This study integrates the findings from cone penetration tests (CPT) with the results of the shaking table tests to assess the liquefaction susceptibility of the sandy copper tailings. In this study, the cone penetration resistance q_c in the sandy copper tailings were found from CPTs conducted using two calibration chambers, one at UNSW and one at The University of Western Australia (UWA). A detailed description of the chambers can be found in Pournaghiazar et al. (2011) and Ayala et al. (2020). Additional q_c were also obtained from CPTs conducted in the tailings models shaken on the shaking table, before and after the shaking events. CPTs conducted in the shaking table models and calibration chambers were saturated and under drained conditions. The CPT results can be found in Jimenez (2024).

5.1 *The critical state framework and triaxial results*

The critical state framework (Jefferies & Been 2015) is used in this study. This is a theoretical state at which the soil will continue to deform at a constant volume under constant shear stress. The model parameters for this framework are typically determined by fitting the results of drained and undrained triaxial compression shearing tests to a mathematical model. Conventional notation is used. $p' = (\sigma_1' + 2\sigma_3')/3$ is the mean effective stress and $q = \sigma_1' - \sigma_3'$ is the deviatoric stress, where σ_1' and σ_3' are the axial and radial effective stresses, respectively.

The mean effective stress is defined as

$$p' = p - u_w \tag{2}$$

where p is the mean total stress and u_w is the pore water pressure. The critical state line (CSL) is defined by a straight line in the $e - \ln p'$ plane, where e is the void ratio, and controlled by the interception with $p' = 1$ kPa, Γ and slope λ.

$$e = \Gamma - \lambda \ln p' \tag{3}$$

The critical state line in the $q - p'$ plane is assumed to be a straight line with a slope M_{cs} according to

$$M_{cs} = \frac{6 \sin \phi_{cs}'}{3 - \sin \phi_{cs}'} \tag{4}$$

where ϕ_{cs}' is the critical state friction angle. In this study, seven triaxial (compression) shear tests on the copper tailings were conducted and the results were fitted to the critical state framework, these results are shown in Figure 7.

Using Equation (3), triaxial testing revealed that the CSL can be defined by $\Gamma = 1.01$, $\lambda = 0.054$ and $M_{cs} = 1.45$.

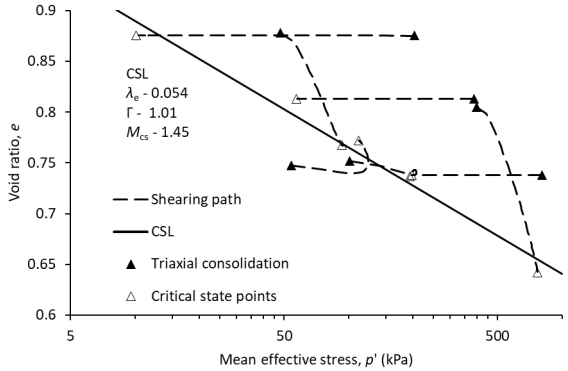

Figure 7. CSL for saturated copper tailings. Also shown are the consolidation and end points of triaxial compression tests used to determine the line locations.

5.2 *CPT interpretation*

The calibration chamber and shaking table CPTs were conducted at a rate slow enough to ensure drained conditions prevail. The state parameter ψ, being the vertical distance between the current e and the e_{cs} on the current CSL (Been & Jefferies 1985), was plotted against the normalised cone resistance $\frac{q_c - p_0}{p'_0} + 1$ (on a log scale) in Figure 8. CPT results of tailings under drained conditions show a unique relationship when plotted in this plane (Been et al. 1986).

$$\frac{(q_c - p_0)}{p_0'} + 1 = \bar{k} \exp(-\bar{m}\psi) \tag{5}$$

in which $\bar{k}$ and $\bar{m}$ are positive dimensionless constants. $\bar{k}$ = 71.6 and $\bar{m}$ = 4.72 apply to the copper tailings as shown in Figure 8.

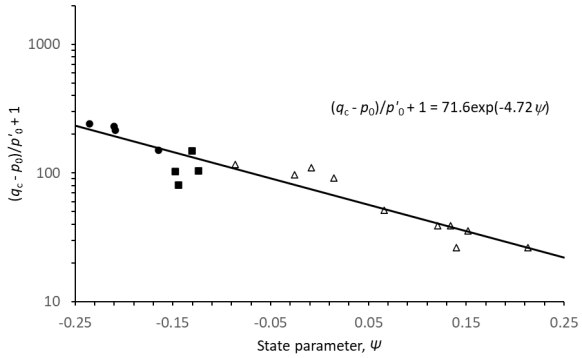

Figure 8. Normalised cone resistance $\frac{(q_c - p_0)}{p_0'} + 1$ against ψ for saturated sandy copper tailings. Solid circular symbols represent data from the shear stack at UNSW. Solid square symbols represent data from the calibration chamber at UNSW. Hollow triangular symbols are from the CPTs conducted on the calibration chamber at UWA.

6 THE LINKAGE BETWEEN ψ AND CSR

The linkage between ψ and CSR establishes a good correlation to assess the liquefaction susceptibility of the copper tailings with the critical state framework. In this research, multiple cyclic direct simple shear (CDSS) tests were performed on the copper tailings to find its CSR with varying ψ and σ'_v. This correlation will then be used to assess its liquefaction susceptibility using the shaking table test results.

6.1 *The cyclic direct simple shear (CDSS) test*

During laboratory testing, fabric characteristics will manifest as a consequence of the chosen sample preparation procedure (Jefferies & Been 2015). Therefore, to minimise differences

between CSR in the shaking table and CDSS tests a similar sample preparation was used.

During the CDSS test, the specimen is sheared cyclically by displacing the lower platen of the device horizontally at a constant rate while the upper platen remains stationary. This simulates the cyclic shear stresses experienced by the tailings during earthquakes or wave loading. The cyclic loading was applied at various stress ratios ($\frac{\tau}{\sigma'_v}$) to investigate the effect of these parameters on soil behaviour.

6.2 *The CDSS results and their link to ψ*

The CDSS results for the copper tailings at different initial conditions, including the adopted CSR and the corresponding number of cycles (N) to achieve liquefaction as well as e_c and ψ, can be found in Jimenez (2024). ψ was calculated using the CSL parameters of the copper tailings as previously detailed in Section 5. Samples were categorised into distinct groups based on their average ψ values to facilitate its linkage to CSR.

Figure 9 illustrates the relationship between cyclic stress ratio CSR and N based on the liquefaction triggering criterion, r_u = 0.9. The data suggest a strong correlation between liquefaction resistance and ψ. The contractive and dilative behaviour of the tailings is effectively captured by ψ and properly represented in Figure 9.

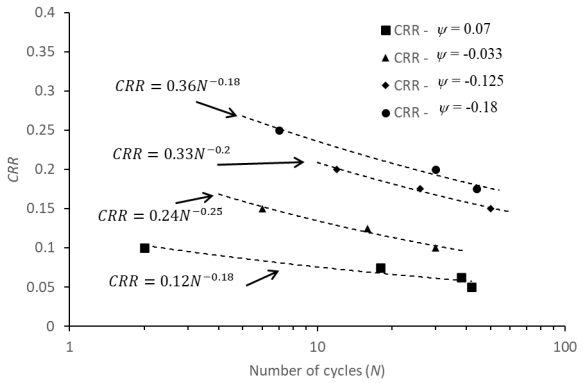

Figure 9. CDSS test results and liquefaction resistance of the copper tailings with varying ψ.

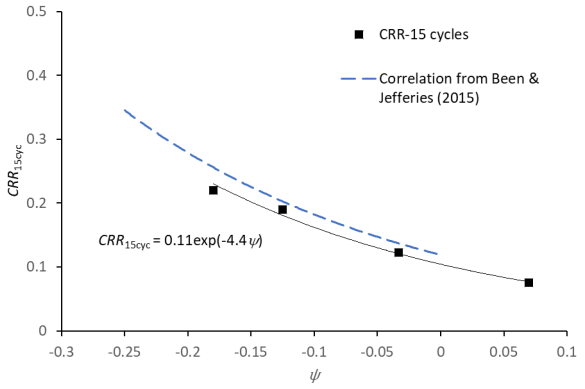

Figure 10. CRR_{15} as a function of ψ for the copper tailings.

Based on the CDSS results in Figure 9 a correlation between CRR and ψ can be established similar to the trend proposed in Figure 8. This new relationship is of the form

$$CRR_{15cyc} = \bar{k}_{CRR} \exp(-\bar{m}_{CRR}\psi) \quad (6)$$

where CRR_{15cyc} is the cyclic resistance ratio for 15 cycles, and both $\bar{k}_{CRR}$ and $\bar{m}_{CRR}$ are dimensionless constants. $\bar{k}_{CRR}$ = 0.11 and $\bar{m}_{CRR}$ = 4.4 apply for the copper tailings as shown in Figure 10.

7 LIQUEFACTION TRIGGERING AND CRR FROM THE SHAKING TABLE TESTS

In this study the process of establishing the CRR values from the non-uniform pulses in the shaking table test involves three stages: (1) Converting the stress-strain time histories into CSR time series, (2) transforming the non-uniform CSR time series into standardised uniform CSR time series, and (3) determining the timing of liquefaction (with $r_u \geq 0.9$ as the triggering criteria) to convert CSR values into CRR values. These stages and the process of conversion are thoroughly explained in Jimenez (2024), including a correction factor considered for non-sinusoidal waves in the CSR time series.

8 CRR_{15CYC} AND LIQUEFACTION ASSESSMENT USING THE CRITICAL STATE APPROACH

CRR_{15cyc} values were obtained at different depths from non-uniform CSR pulses using the procedure described in Section 7. The complete CSR time series was converted to CRR_{15cyc} when the tailings didn't liquefy, i.e. for PGA 0.08 g and 0.1 g. When the tailings liquefied, CRR_{15cyc} values were calculated from the CSR loading up to the time of liquefaction $r_u \geq 0.90$ with data obtained from the piezometers. Here, CRR_{15cyc} values are presented from the layers next to the accelerometers A1 and A4 (0.1 and 0.4 m from the base, respectively) since they show the least and most liquefiable layer in the two tailings models for all the shaking pulses. For example, for a PGA of 0.1 g in the first model, where no liquefaction occurs in neither A1 nor A4, CRR_{15cyc} is calculated from the complete CSR time series resulting in CRR_{15cyc} values of 0.19 at 0.28 m depth (A4) and 0.186 at 0.58 m depth (A1). For a PGA of 0.14 g in the first model, where liquefaction occurs after 4.2 s at 0.28 m depth and after 5.0 s at 0.58 m depth, as shown in Figure 6, CRR_{15cyc} is calculated from the conversion of the CSR up to the triggering time resulting in CRR_{15cyc} values of 0.286 at 0.28 m depth (A4) and 0.264 at 0.58 m depth (A1).

A summary of the experimental results obtained from the shaking table test including CRR_{15cyc}, e, ψ and q_c are presented in Table 3 and Table 4. ψ was calculated using the CSL parameters of the copper tailings as previously detailed in Section 5.2. Also, q_c is associated to ψ through $\frac{(q_c - p_0)}{p'_0} + 1 = \bar{k}\exp(-\bar{m}\psi)$ for each shaking event.

Table 3. Summary of the shaking table test results considering CRR_{15cyc}, e, ψ and q_c for the different PGAs in the first model.

PGA (g)	CRR_{15cyc} A1	CRR_{15cyc} A4	e	ψ	p'_0 (kPa)	q_c (MPa)
0.08	0.151	0.156	0.735	-0.187	4.24	0.74
0.10	0.186	0.190	0.733	-0.189	4.24	0.75
0.12	0.240	0.254	0.728	-0.194	4.24	0.77
0.14	0.264	0.286	0.726	-0.196	4.24	0.78
0.16	0.330	0.303	0.703	-0.219	4.23	0.86
0.20	0.409	0.351	0.675	-0.247	4.22	0.98
0.30	0.511	0.408	0.658	-0.264	4.21	1.06

Table 4. Summary of the shaking table test results considering CRR_{15cyc}, e, ψ and q_c for the different PGAs in the second model.

PGA (g)	CRR_{15cyc} A1	CRR_{15cyc} A4	e	ψ	p'_0 (kPa)	q_c (MPa)
0.08	0.112	0.086	0.861	-0.059	4.37	0.42

0.10	0.143	0.111	0.859	-0.061	4.37	0.43
0.12	0.200	0.158	0.855	-0.066	4.37	0.44
0.14	0.241	0.178	0.844	-0.077	4.36	0.46
0.16	0.233	0.207	0.809	-0.111	4.35	0.54
0.20	0.292	0.226	0.783	-0.137	4.34	0.60
0.30	0.390	0.333	0.749	-0.172	4.32	0.71

The CRR_{15cyc} values from the shaking table test are used with its corresponding e or ψ, obtained from the initial height and subsequent settlements of the tailings bed before each shaking event, to assess the liquefaction susceptibility of the copper tailings by proposing a new numerical relationship between CRR_{15cyc} and q_c.

By using the relationship between q_c and ψ in Equation (5), and the relationship between CRR_{15cyc} and ψ in Equation (6), the following interrelationship between CRR_{15cyc} and q_c can be found and is of the form

$$CRR_{15cyc}=\bar{k}_{CRR}\left(\frac{(q_c - p_0)/p'_0 + 1}{\bar{k}}\right)^{\bar{m}_{CRR}/\bar{m}} \quad (7)$$

where $\bar{k}$ = 71.6, $\bar{m}$ = 4.72, $\bar{k}_{CRR}$ = 0.11 and $\bar{m}_{CRR}$ = 4.4 apply for the copper tailings. p_0 and p'_0 are the total mean stress and mean effective stress, respectively, at the specific depth of liquefaction assessment within the tailings bed.

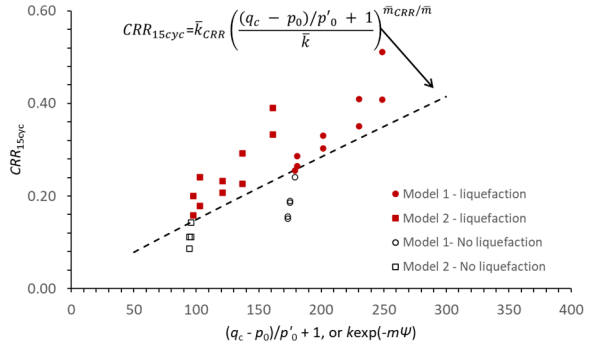

Figure 11. CRR_{15cyc} plotted against $(q_c - p_0)/p'_0 + 1$, or $\bar{k}\exp(-\bar{m}\psi)$ for the copper tailings results in the biaxial shaking table test. CRR_{15cyc} values when liquefaction occurred, from models 1 and 2, are plotted as solid red symbols, and CRR_{15cyc} when liquefaction did not occur are plotted as hollow symbols. The calculated liquefaction line is also shown as a dashed line.

Figure 11 shows the CRR_{15cyc} values obtained from the shaking table tests and compared them against the numerically calculated liquefaction triggering curve in Equation (7). A strong agreement is shown between the experimentally obtained CRR_{15cyc} and the calculated liquefaction triggering curve separating the CRR_{15cyc} values where liquefaction did not occur from the ones where liquefaction occurred.

9 CONCLUSIONS

Multiple shaking table tests were conducted on the copper tailings, using two different physical models, to examine its liquefaction susceptibility. The cyclic strength, based on the cone penetration resistance, was assessed using a critical state soil mechanics approach. Data from accelerometers were used to calculate the cyclic stress ratio induced during the shaking events. Cone penetration tests conducted in the UNSW calibration chamber, UNSW shear stack and UWA chamber were used to propose a correlation between $\frac{q_c - p_0}{p'_0} + 1$ and ψ. The correlation was then used to relate q_c to CRR_{15cyc}. Calculation of CRR_{15cyc} from the experimental data was highly dependent on the timing on liquefaction.

A new framework enabling the possibility of liquefaction to be determined for the copper tailings has been presented. A strong agreement has been found between the numerically calculated liquefaction triggering curve and the experimentally obtained CRR_{15cyc} from the shaking table tests. This methodology holds significant potential for advancing empirical procedures in estimating the consequences of soil or tailings liquefaction.

While the findings in this chapter are encouraging, further research involving a wider range of soil and tailings types is needed to expand the applicability of this proposed framework.

10 ACKNOWLEDGEMENTS

Part of this work stems from TAILLIQ (Tailings Liquefaction), which is an Australian Research Council (ARC) Linkage Project (LP160101561) supported by financial and in-kind contributions from Anglo American, BHP, Freeport-McMoRan, Newmont, Rio Tinto and Teck. The TAILLIQ project is being carried out at The University of New South Wales, The University of South Australia, The University of Western Australia (lead organisation) and The University of Wollongong. We acknowledge the support and contributions of project personnel at each of the supporting organisations. The work also forms part of an ARC Future Fellowship award (FT200100820) and that funding is gratefully acknowledged.

11 REFERENCES

Ayala, J., Fourie, A. and Reid, D., 2020. Cone penetration testing on silty tailings using a new small calibration chamber. *Geotechnique Letters*, 10(4), pp.492–497.

Been, K., Crooks, J.H.A., Becker, D.E. and Jefferies, M.G., 1986. The cone penetration test in sands: Part I, state parameter interpretation. *Geotechnique*, 36(2), pp.239–249.

Been, K. and Jefferies, M.G., 1985. A state parameter for sands. *Geotechnique*, 35(2), pp.99–112.

Darby, K.M., Boulanger, R.W., DeJong, J.T. and Bronner, J.D., 2019. Progressive Changes in Liquefaction and Cone Penetration Resistance across Multiple Shaking Events in Centrifuge Tests. *Journal of Geotechnical and Geoenvironmental Engineering*, 145(3).

Fourie, A.B., Blight, G.E. and Papageorgiou, G., 2001. Static liquefaction as a possible explanation for the Merriespruit tailings dam failure. *Canadian Geotechnical Journal*, 38(4), pp.707–719.

Jefferies, M. and Been, K., 2015. *Soil liquefaction: A critical state approach*. CRC Press.

Jimenez, A., 2024. *CPT results in and liquefaction of variably saturated tailings*. PhD Thesis. UNSW.

Koga, Y. and Matsuo, O., 1990. Shaking Table Tests of Embankments Resting on Liquefiable Sandy Ground. *Soils and Foundations*, 30(4), pp.162–174.

Pournaghiazar, M., Russell, A.R. and Khalili, N., 2011. Development of a new calibration chamber for conducting cone penetration tests in unsaturated soils. *Canadian Geotechnical Journal*, 48(2), pp.314–321.

Robertson, P.K., de Melo, L., Williams, D.J. and Wilson, G.W., 2019. *Report of the expert panel on the technical causes of the failure of Feijão dam I. Commissioned by Vale*.

Tiwari, R., Jimenez, A. and Russell, A.R., 2024. A novel biaxial shaking table and its performance when investigating seismic actions. *Earthquake Engineering & Structural Dynamics*.

Yazdandoust, M., 2017. Investigation on the seismic performance of steel-strip reinforced-soil retaining walls using shaking table test. *Soil Dynamics and Earthquake Engineering*, 97, pp.216–232.

Zeghal, M., Elgamal, A.W., Zeng, X. and Arulmoli, K., 1999. Mechanism of liquefaction response in sand-silt dynamic centrifuge tests. *Soil Dynamics and Earthquake Engineering*, 18(1), pp.71–85.